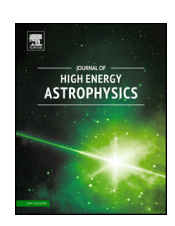
ELSEVIER

Contents lists available at ScienceDirect

Journal of High Energy Astrophysics

www.elsevier.com/locate/jheap



An explanation of the muon puzzle of ultrahigh-energy cosmic rays and the role of the Forward Physics Facility for model improvement



Luis A. Anchordoqui ^{a,b,c,*}, Carlos García Canal ^d, Felix Kling ^e, Sergio J. Sciutto ^d, Jorge F. Soriano ^a

- ^a Department of Physics and Astronomy, Lehman College, City University of New York, NY 10468, USA
- ^b Department of Physics, Graduate Center, City University of New York, NY 10016, USA
- ^c Department of Astrophysics, American Museum of Natural History, NY 10024, USA
- d Instituto de Física La Plata CONICET and Departamento de Física, Facultad de Ciencias Exactas, Universidad Nacional de La Plata, C.C. 69, (1900) La Plata, Argentina
- e Deutsches Elektronen-Synchrotron DESY, Notkestr. 85, 22607 Hamburg, Germany

ARTICLE INFO

ABSTRACT

Article history: Received 16 March 2022 Accepted 22 March 2022 We investigate the observed muon deficit in air shower simulations when compared to ultrahighenergy cosmic ray (UHECR) data. Based upon the observed enhancement of strangeness production in high-energy hadronic collisions reported by the ALICE Collaboration, the concomitant $\pi \leftrightarrow K$ swap is considered as the keystone to resolve the muon anomaly through its corresponding impact on the shower development. We construct a toy model in terms of the $\pi \leftrightarrow K$ swapping probability F_s . We present a parametrization of F_s in terms of the pseudorapidity that can accommodate the UHECR data. Looking to the future, we explore potential strategies for model improvement using the massive amounts of data to be collected by LHC neutrino detectors, such as FASER ν and experiments at the Forward Physics Facility. We calculate the corresponding sensitivity to F_s and show that these experiments will be able to probe the model phase space.

© 2022 Elsevier B.V. All rights reserved.

1. Introduction

Ultra-high-energy ($10^9 \lesssim E/\text{GeV} \lesssim 10^{11}$) cosmic ray (UHECR) collisions have center-of-mass energies ($50 \lesssim \sqrt{s}/\text{TeV} \lesssim 450$) well beyond those achieved at collider experiments, and thereby provide an invaluable probe of particle interactions below the Fermi distance (Anchordoqui, 2019). Of particular interest here, the highest energy cosmic rays currently observed by the Pierre Auger Observatory (Auger) (Aab et al., 2015, 2016a) and the Telescope Array (Abbasi et al., 2018) show a significant discrepancy in the shower muon content when compared to predictions of LHC-tuned hadronic event generators (d'Enterria et al., 2011). More concretely, the analysis of Auger data suggests that the hadronic component of showers (with primary energy $10^{9.8} < E/\text{GeV} < 10^{10.2}$) contains about 30% to 60% more muons than expected. The significance of the discrepancy between Auger data and model prediction is somewhat above 2.1σ (Aab et al., 2016a). Auger findings have been recently confirmed studying air shower measurements over a wide range of energies. The muon deficit between simulation and data, dubbed the *muon puzzle*, starts at $E \sim 10^8$ GeV increasing noticeably as primary energy grows, with a slope which was found to be significant at about 8σ (Dembinski et al., 2021).

Certainly, in solving the muon puzzle one has to simultaneously get a good agreement with the measurements of the distribution of the depth of shower maximum, X_{max} , and the fluctuations in the number of muons (Aab et al., 2021). A thorough phenomenological study has shown that an unrivaled solution to the muon deficit, compatible with the observed X_{max} distributions, is to reduce the transfer of energy from the hadronic shower into the electromagnetic shower, by reducing the production or decay of neutral pions (Allen and Farrar, 2013). Several models have been proposed to accommodate this effect, including those wherein strangeness production suppresses the pion-to-kaon ratio (Farrar and Allen, 2013; Anchordoqui et al., 2017; Baur et al., 2019). This modification could have a compounded effect on the hadronic cascade, so that only a comparably small reduction of π^0 production is required.

E-mail address: luis.anchordoqui@gmail.com (L.A. Anchordoqui).

^{*} Corresponding author.

We note in passing that the proposed enhancement of strangeness production in high-energy hadronic collisions was observed by ALICE in the mid-rapidity region (Adam et al., 2017), Specifically, ALICE observations show an enhancement of the yield ratio of strange and multi-strange hadrons to charged pions as a function of multiplicity at mid-rapidity not only in PbPb and XeXe collisions but also in pp and pPb scattering (Palni, 2019). It goes without saying that none of the hadronic interaction models currently used in air shower simulations correctly reproduce the main tendencies of ALICE data (Anchordogui et al., 2020), Assuming that the observed enhancement of strangeness production in high-energy hadronic collisions is at the core of the muon puzzle in this paper we study the concomitant $\pi \leftrightarrow K$ swap impact on the development of extensive air showers (EASs), using phenomenological toy models implemented in AIRES (version 19.04.08) (Sciutto, 1999). After that, we discuss the prospects to constrain our model using forward neutrino flux measurements at FASERy (Abreu et al., 2020, 2001) and future experiments at the Forward Physics Facility (FPF) (Anchordogui et al., 2021).

There are two points worth noting at this juncture: (i) The mid-rapidity region in which the ALICE Collaboration reported a universal strangeness enhancement in pp, pPb and PbPb collisions is not directly relevant for air showers experiments. It has not been observed experimentally yet whether these effects could also be seen in hadrons produced at forward rapidities. This is the main assumption of our model, which will be directly tested at the FPF. (ii) Accommodating the muon deficit between simulations and data can be virtually reduced to a constant factor, which is independent of the primary energy (Sciutto, 2019). In our toy model this factor is taken to be related to the $\pi \leftrightarrow K$ swapping probability.

The layout of the paper is as follows. In Sec. 2 we first discuss general aspects of a toy model and describe the (input and output) AIRES module interface. Armed with the new AIRES module we confront the toy model with Auger data. We perform a parameter scan using results of EAS simulations and determine the phase space boundaries of the $\pi \leftrightarrow K$ swapping probability from experimental data. In Sec. 3 we improve our toy model to transform it into a predictive model. We present a parametrization of the $\pi \leftrightarrow K$ swapping probability in terms of the pseudorapidity that can accommodate the UHECR data. In Sec. 4 we investigate the sensitivity to the $\pi \leftrightarrow K$ swapping probability at FASER v and the FPF and demonstrate that a direct test of the model predictions is indeed feasible. The paper wraps up with some conclusions presented in Sec. 5.

2. A toy model

To describe the shower evolution we adopt the AIRES simulation engine (Sciutto, 1999) which provides full space-time particle propagation in a realistic environment. The features of the AIRES version used for this work (19.04.08) are explained in detail in Sciutto

For the present analysis, we prepared a new module to account for the possible enhancement of strangeness production in high-energy hadronic collisions. Every time an hadronic collision is processed, the list of secondary particles obtained from the external event generator invoked (for our analysis we adopt SIBYLL 2.3d (Riehn et al., 2020)) is scanned by the new module before passing it to the main particle propagating engine. The main characteristics of the new AIRES module are as follows.

2.1. Model parameters

Swapping fraction	f_s	Controls the kind and number of secondary particles that are affected by change of identity: $-1 \le f_s \le 1$. In this zeroth-order approximation we take the swapping probability $F_s = f_s$.
Projectile energy range	$[E_{pmin}, E_{pmax}]$	Particle swapping is performed only in hadronic collisions where the projectile kinetic energy verifies $E_{\rm pmin} \leq E_{\rm proj} < E_{\rm pmax}$. $E_{\rm pmin}$ must be larger than 900 MeV and less than $E_{\rm pmax}$. We set $E_{\rm pmax} \rightarrow \infty$ unless otherwise specified.
Secondary energy range	$[E_{\rm smin}, E_{\rm smax}]$	Secondary particles with kinetic energies out of the range $[E_{smin}, E_{smax}]$ are always left unchanged. E_{smin} must be larger than 600 MeV and less than E_{smax} . We set $E_{smin} = 1$ TeV, and $E_{smax} \rightarrow \infty$ unless otherwise specified.

2.2. Logics of hadronic collision post-processing

During shower simulation, hadronic collisions are processed via calls to an event generator; we adopt SIBYLL 2.3d (Riehn et al., 2020). The input parameters for these calls are the projectile identity $p_{\rm id}$, its kinetic energy $E_{\rm proj}$, and the target identity. On return, the generator provides a list of N_{sec} particles, specifying their identity s_{id_i} , energy E_{sec_i} , momentum, etcetera, with $i = 1, \dots, N_{\text{sec}}$.

All the returned secondary particle lists undergo a post-processing process, just before they are stacked into the particle stacks for further propagation. The post-processing algorithm obeys the following rules:

```
1. If f_s = 0 or E_{proj} < E_{pmin} or E_{proj} > E_{pmax} then no action is taken; the secondary particle list remains unchanged.
2. If f_s \neq 0 and E_{pmin} \leq E_{proj} \leq E_{pmax} then the list of secondaries is scanned, and processed as follows:
```

- (a) If $f_s > 0$, all the secondary pions whose kinetic energies lie within the interval $[E_{smin}, E_{smax}]$ are considered for identity swapping. Each of them is randomly selected with probability $|f_s|$. In case of positive selection, the identity is changed with the following
 - i. Each π^0 is transformed onto K^0_S of K^0_L , with 50% chance between them. ii. Each π^+ (π^-) is transformed onto K^+ (K^-).

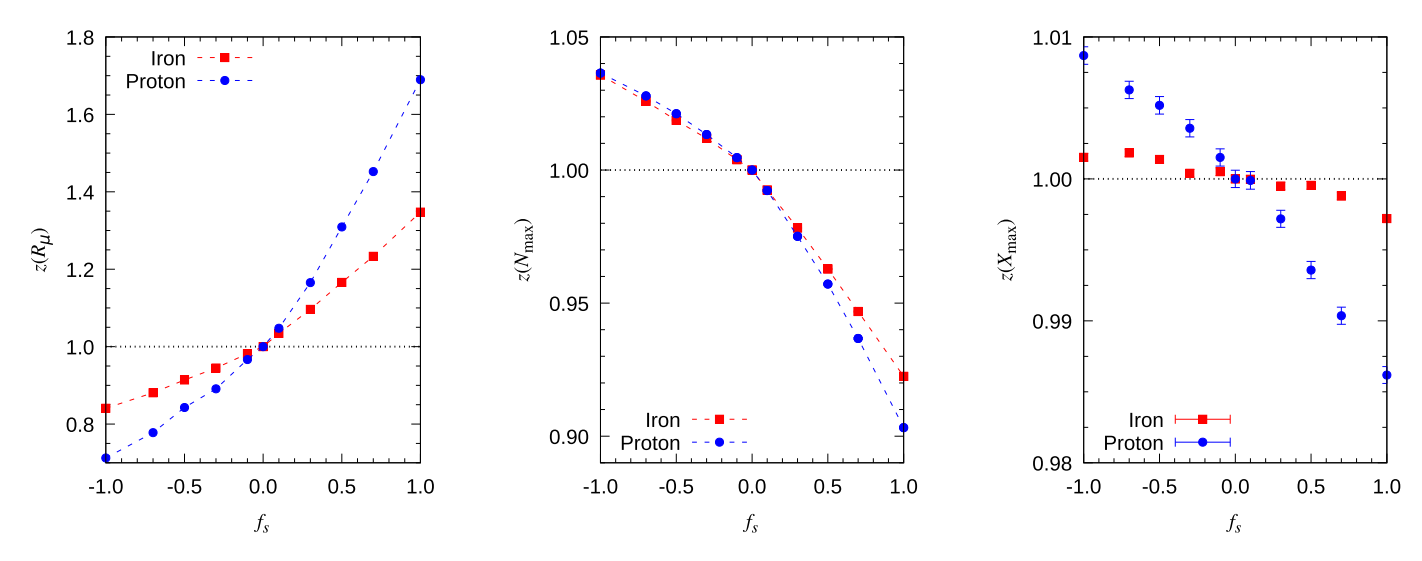


Fig. 1. $z(R_{\mu})$, $z(N_{\text{max}})$, and $z(X_{\text{max}})$ as a function of f_s , for $E_{\text{proj}} = 10$ EeV, $E_{\text{smin}} = 1$ TeV, and $E_{\text{pmin}} = 1$ PeV. We have run 1600 (20000) showers per point for ground muons (longitudinal development), setting at each case the thinning algorithm parameters to get a more detailed simulation of the hadronic or the electromagnetic cascade, respectively.

- (b) If $f_s < 0$, all the secondary kaons whose kinetic energies lie within the interval $[E_{smin}, E_{smax}]$ are considered for identity swapping. Each of them is randomly selected with probability $|f_s|$. In case of positive selection, the identity is changed with the following criterion:
 - i. Each K_S^0 or K_L^0 is transformed onto π^0 . ii. Each K^+ (K^-) is transformed onto π^+ (π^-).
- 3. The kinetic energy of swapped particles is set so as to keep total energy conserved.

2.3. Air shower simulations

To characterize the possible cross-correlation among selected observables we have simulated more than a million showers with incident zenith angles of 45° and 67°. The shower observables relevant to our analysis are:

- the depth of maximum shower development X_{max} and its fluctuations σX_{max} ; the dimensionless muon content $R_{\mu} = N_{\mu}/N_{\mu,19}$ and its fluctuations σR_{μ} , where N_{μ} is the total number of muons (with $E_{\mu} > 10^{-10}$). 300 MeV) at ground level and $N_{\mu,19} = 1.455 \times 10^7$ is the average number of muons in simulated proton showers at 10^{19} eV with incident angle of 67°;
- the number of charged particles at the shower maximum N_{max} .

For each observable \mathcal{O} , we evaluate

$$z(\mathcal{O}) = \frac{\langle \mathcal{O}(f_s) \rangle}{\langle \mathcal{O}(f_s = 0) \rangle},\tag{1}$$

to work with normalized variables.

In Fig. 1 we show $z(R_{\mu})$, $z(N_{\text{max}})$, and $z(X_{\text{max}})$, as a function of f_s , for E=10 EeV, $E_{\text{smin}}=1$ TeV, and $E_{\text{pmin}}=1$ PeV, with both $E_{\text{smax}}=1$ and $E_{\rm pmax}$ set to infinite. Note that this particular $E_{\rm pmin}$ corresponds to hadronic interactions at $\sqrt{s_{NN}} \approx 1.41$ TeV, just below the energy $(\sqrt{s_{NN}}|_{\text{ALICE}} \simeq 2.76 \text{ TeV})$ where the ALICE Collaboration reported a smooth rise of the hyperon-to-pion ratio (Abelev et al., 2014). Note also that for $f_s < 0$, kaons are changed into pions, whereas for $f_s > 0$, pions are changed into kaons, with progressive probability equal to $|f_s|$. The simulations to evaluate X_{max} are always carried out using inclined showers at 45°. The variations in X_{max} fluctuations (not shown in the figure) are very small: $|z(\sigma X_{\text{max}}) - 1| < 0.03$ for all $f_s \in [-1, 1]$. Taking $f_s \sim 0.4$ as fiducial we observe a change in R_{μ} of roughly 20% for showers initiated by protons and 10% in those initiated by iron. These variations correspond to a reduction of N_{max} by about 3%. In the right panel of Fig. 1 we can see that the model predictions on X_{max} vary less than 1.5% when compared to the $f_s = 0$ result. Similarly, the fluctuations σX_{max} vary by less than 3%. Our analysis thus corroborates the results presented in Allen and Farrar (2013), which show that by suppressing the π^0 energy fraction we can obtain an increase in the number of muons at ground without coming into conflict with X_{max} observations.

To study the model dependence with $E_{\rm smin}$ and $E_{\rm pmin}$ we use proton induced showers. In Fig. 2 we show the dependences of R_{μ} and N_{max} with E_{smin} (upper row) and E_{pmin} (lower row). We can see that the change of E_{smin} leads to negligible effects, and that there is virtually no difference between $E_{pmin} = 90$ GeV and $E_{pmin} = 10$ TeV, indicating a saturation effect; see Appendix A. These are, however, unrealistic energy thresholds. A linear dependence between the two observables is evident, especially for $z(R_{\mu}) \sim 1$. The physically unrealistic case of $E_{pmin} = 90$ GeV is the one that presents the largest departure from linearity.

In the spirit of Sciutto (2019), we now incorporate the change of the nuclear composition of the cosmic ray primary (Aab et al., 2017) and study the variation of $\langle R_{\mu} \rangle / (E/10 \text{ EeV})$. As displayed in Fig. 3, the effect of increasing R_{μ} yields a flattening of the curve when

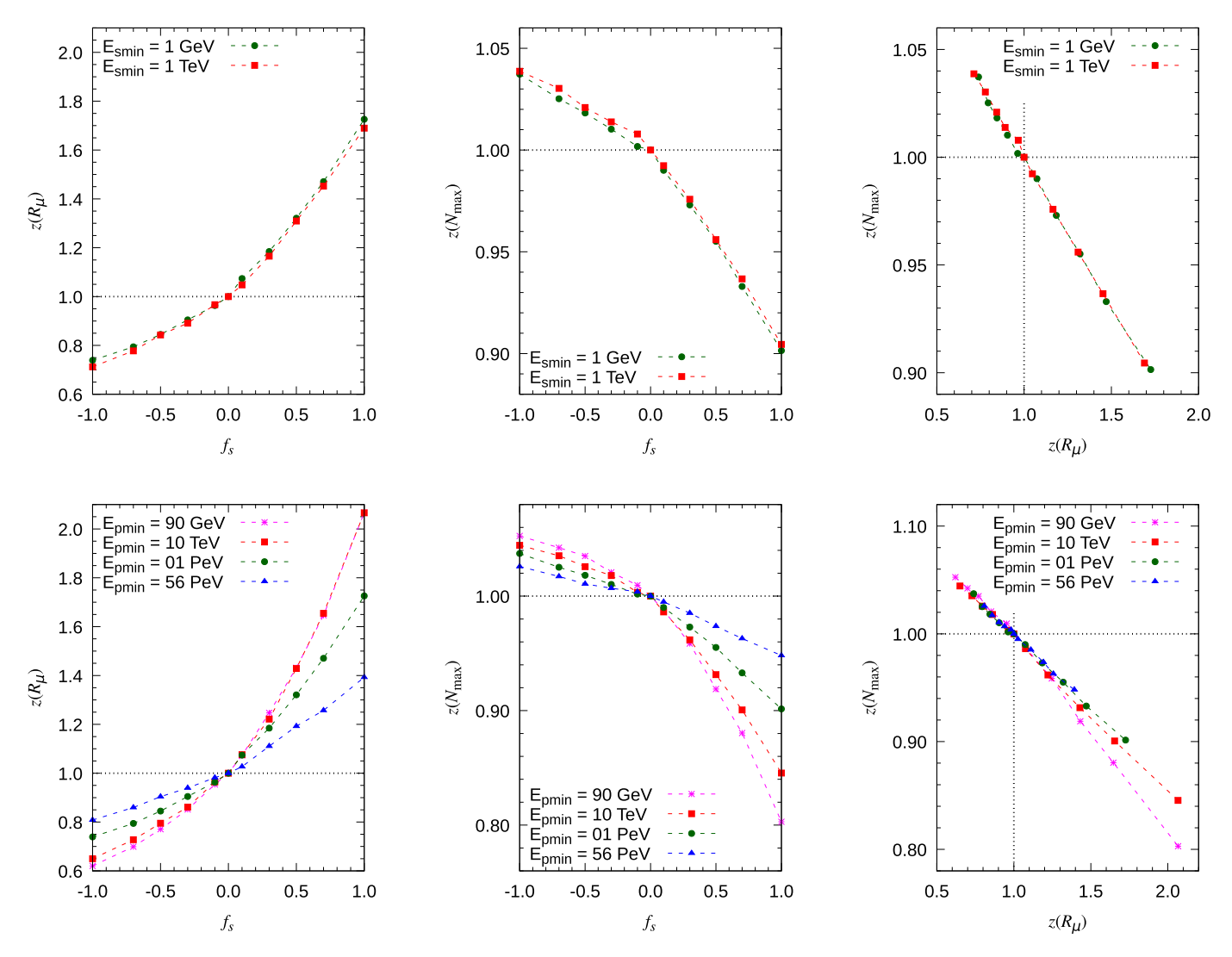


Fig. 2. $z(R_{\mu})$ versus f_s (left), $z(N_{\text{max}})$ versus f_s (middle), and $z(R_{\mu})$ versus $z(N_{\text{max}})$ (right), for varying E_{smin} (upper), and E_{pmin} (lower).

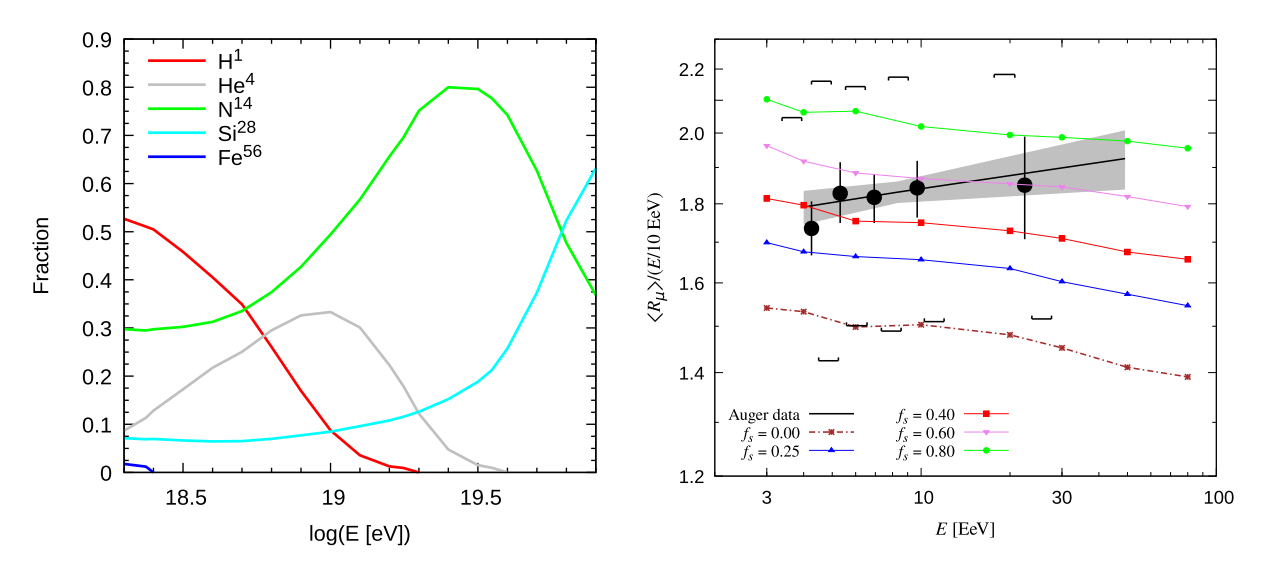


Fig. 3. Left. Fractions of ultra-high energy primary cosmic rays entering at the top of the Earth's atmosphere, as functions of the primary energy, evaluated from partial fluxes corresponding to the fit reported by the Pierre Auger Collaboration (Aab et al., 2017). **Right.** Estimations of R_{μ} from AIRES + SIBYLL 2.3d simulations for different values of f_s superimposed over Auger data with statistical (ϕ) and systematic (ϕ) uncertainties (Aab et al., 2015). We have adopted the mixed baryonic composition shown in the left panel.

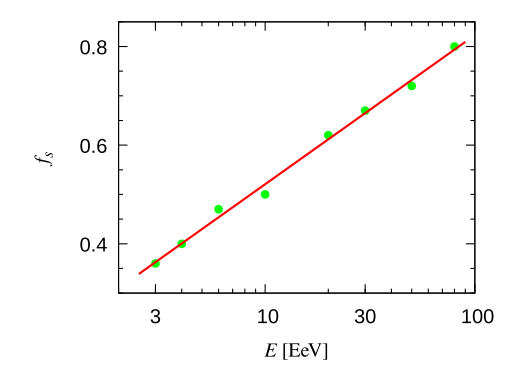


Fig. 4. Variation of f_s with energy as determined from eyeball fitting the rising straight-line R_μ estimation of Fig. 3.

compared to the $f_s = 0$ prediction. Even though $f_s \sim 0.4$ seems to roughly accommodate the data around $E \sim 10^{19}$ eV, it is clear from the shape of the best-fit curve that to describe the muon anomaly in a larger energy range we would need an energy-dependent f_s ; see Fig. 4.

We note, however, that this zeroth order approximation should be understood as an effective (macroscopic) description of the entire shower evolution, rather than a collection of individual interactions generated by a homogeneous beam of projectiles. In this approach E_{pmin} is no less important than E_{smin} and for a 10¹⁰ GeV proton shower with $f_s = 0.7$ the number of pions effectively swapped barely exceeds 0.5% of the total number of secondaries generated in shower. Global observables, such as the number of muons at ground level, were obtained after adding and averaging heaps of individual contributions, a process in which statistics erases many "microscopic" details.

3. Model refinement

In the previous section we have shown that the zeroth order approximation toy model gives a fair description of all shower observables. However, there are two important caveats with this toy model. Firstly, heavy flavor production should be enhanced in kinematic regimes where quark masses may be insignificant. This implies that a more realistic parametrization of F_s , which can accurately describe single particle collisions, should depend on pseudorapidity. Secondly, the shape of the best-fit curve to Auger data is driven by both strangeness enhancement and the rapid change in the nuclear composition (Sciutto, 2019). Thus, nuclear effects (Anchordoqui et al., 2017) could play a conclusive role in bridging the gap between data and simulations, hinting that F_s should also have a variation with the nucleus baryon number A. Along this line, a strong suppression of the production of neutral pions in pPb collisions was reported by the LHCf Collaboration after comparing to the results of pp scattering (Adriani et al., 2014). Uncertainties on the A dependence of F_s are still quite large, and so for simplicity, we will neglect A-induced effects in our study. Future LHC data (including pO and OO collisions (Citron et al., 2019)) will provide new insights to reduce these uncertainties and guide software development.

The Lorentz transformation between the center-of-mass (CM) and laboratory (LAB) systems is given by

$$E_{\text{LAB}} = \gamma (E_{\text{CM}} + \beta \ p_{\text{long,CM}}), \tag{2}$$

where γ is the Lorentz factor and β the velocity of the CM with respect to the LAB frame. For ultrarelativistic particles, $\beta \sim 1$ and $p_{\text{long,CM}} \sim E_{\text{CM}} \cos \theta_{\text{CM}}$, where θ_{CM} is the angle of the secondary particle's momentum with respect to the axis where the projectile of the collision moves (i.e. direction of the beam). A straightforward substitution leads to

$$E_{\text{LAB}} \sim \gamma \ E_{\text{CM}} \left(1 + \cos \theta_{\text{CM}} \right). \tag{3}$$

At first sight one may conjecture that the imposed lower limit on E_{smin} in our toy model is inconsistent with the description of hadronic collisions as $0 < E_{LAB} < 2\gamma E_{CM}$. To inspect the forward-backward directions in the CM frame we conveniently work with the pseudorapidity

$$\eta_{\rm CM} = -\ln\left[\tan\left(\frac{\theta_{\rm CM}}{2}\right)\right]. \tag{4}$$

The forward-backward symmetry of Eq. (3) is evident in the pion pseudorapidity distributions shown in the upper row of Fig. 5. We note that the toy model approximation $E_{smin}=1$ TeV breaks this symmetry when going into the LAB frame; see the lower row of Fig. 5. In particular, pions with $\eta_{CM}<-4$ are not considered for swapping in the AIRES module described in Sec. 2. The relation between the CM and LAB pseudorapidity is displayed in the scatter plots of Fig. 6. It is important to stress that the densities of dots in different places of these plots may not accurately represent the actual number of secondaries that corresponds to each location within the (η_{LAB} , E_{LAB}) plane. This is due to the fact that to improve the graphics readability, only a small fraction, non-uniformly sampled, of the total number of secondaries produced in the collision has been represented. The sampling was performed trying to obtain a uniform coverage of the entire range of CM pseudorapidities of the secondaries. To this end, the $-\infty < \eta_{CM} < \infty$ axis is partitioned in consecutive intervals, with extremes at the points $-\infty$, -10, -7, -5, -4, -3, -2, 0, 2, 3, 4, 5, 7, 10, ∞ , and then the entire set of secondary pions emerging from the collisions is scanned sampling 100 cases for each one of those intervals. For a realistic appreciation of the distribution of secondary particles, it is better see the bivariate distributions shown in Fig. 5.

As the shower develops in the atmosphere, the hadrons propagate through a medium with an increasing density while the altitude decreases and the hadron-air cross section rises slowly with energy. Thereby, the probability for interacting with the air molecules before decay increases with rising energy. Furthermore, the relativistic time dilation increases the decay length by a factor E_h/m_h , where E_h and

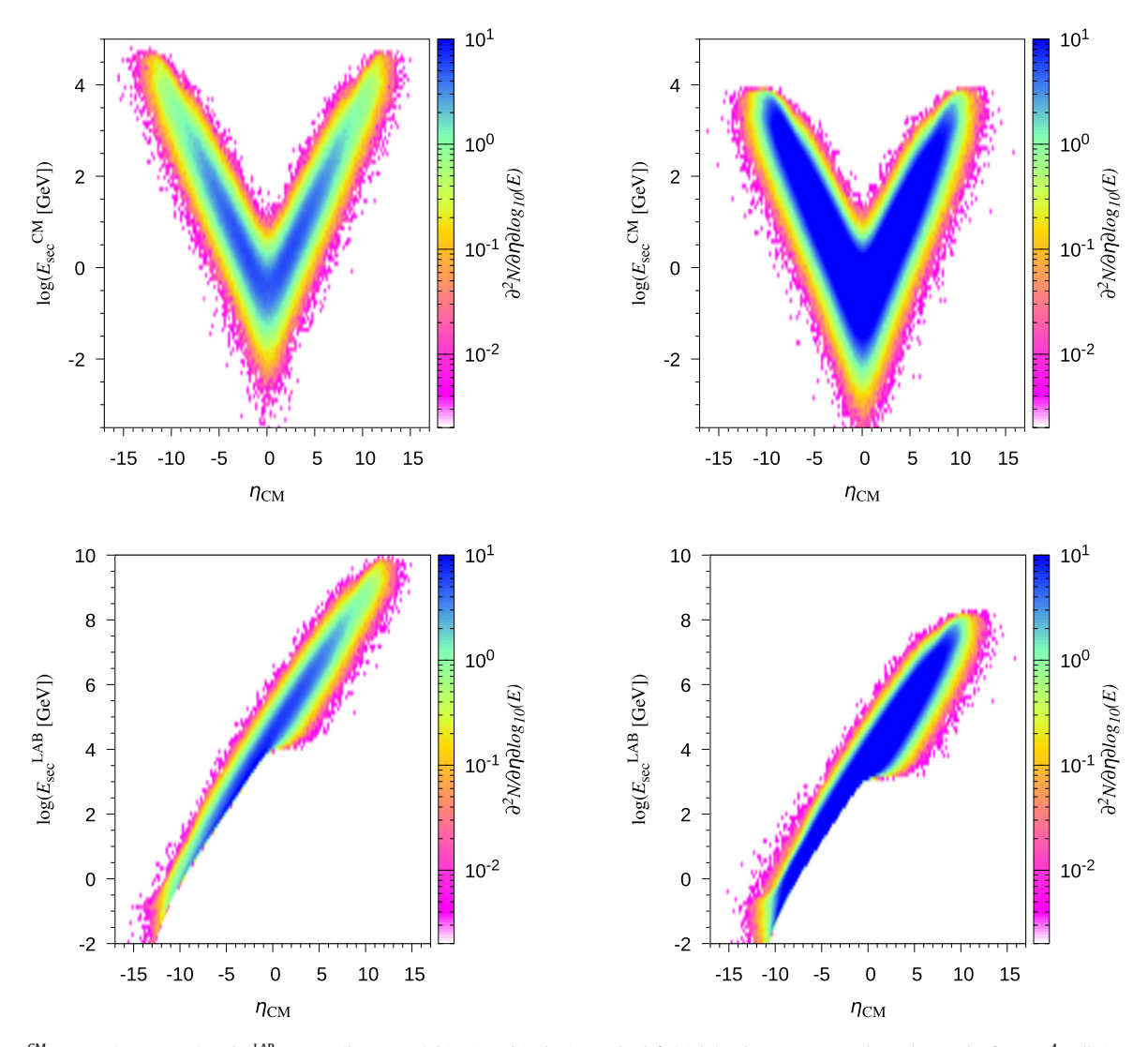


Fig. 5. Pion $E_{\text{sec}}^{\text{CM}}$ vs η_{CM} (upper row) and $E_{\text{sec}}^{\text{LAB}}$ vs η_{CM} (lower row) bivariate distributions. The left (right) column corresponds to the results from 10⁴ collisions of a 10 EeV proton (iron nucleus) scattering off a proton (nitrogen nucleus) at rest, simulated with SIBYLL 2.3d.

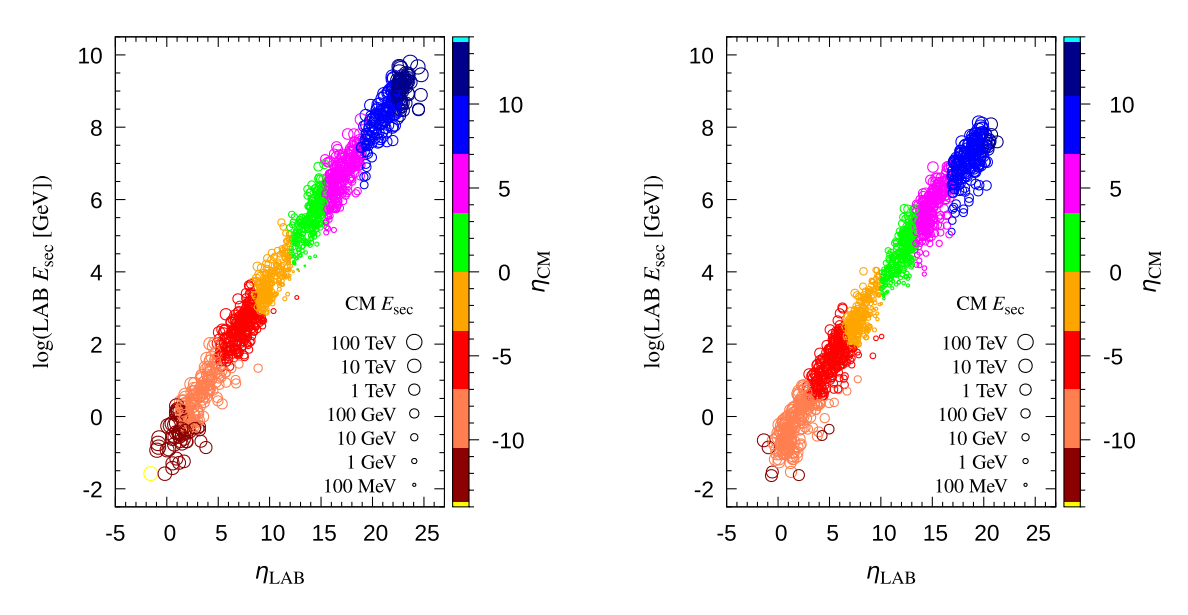


Fig. 6. $E_{\text{sec}}^{\text{LAB}}$ vs η_{LAB} scatter plots for secondary pions generated in 10 EeV collisions of a proton scattering off a stationary proton (left) and an iron nucleus scattering of a nitrogen nucleus (right). The CM pseudorapidity and CM kinetic energy of the secondaries can be appreciated at each plotted dot by means of the dot color and its size, respectively, accordingly with the color scale placed at the right of the plots and size scales indicated in each graph.

 m_h are the energy and mass of the produced hadron. The π^0 's, with a lifetime of $\simeq 8.4 \times 10^{-17}$ s, do decay promptly to two photons, feeding the electromagnetic component of the shower. To see how neutral kaons could suppress this process, it is instructive to estimate the critical energy at which the chances for interaction and decay are equal for other longer-lived mesons. For a vertical transversal of the atmosphere, the critical energy is found to be: $\xi_c^{\pi^\pm} \sim 115$ GeV, $\xi_c^{K^\pm} \sim 850$ GeV, $\xi_c^{K^0_1} \sim 210$ GeV, $\xi_c^{K^0_2} \sim 30$ TeV (Gondolo et al., 1996). The dominant K^+ branching ratios are to $\mu^+\nu_\mu$ (64%), to $\pi^+\pi^0$ (21%), to $\pi^+\pi^+\pi^-$ (6%), and to $\pi^+\pi^0\pi^0$ (2%), whereas those of the K_S^0 are to $\pi^+\pi^-$ (60%), to $\pi^0\pi^0$ (30%), and for K_L^0 we have $\pi^\pm e^\mp \nu_e$ (40%), $\pi^\pm \mu^\mp \nu_\mu$ (27%), $\pi^0\pi^0\pi^0$ (19%), $\pi^+\pi^-\pi^0$ (12%) (Zyla et al., 2020). Using these branching fractions, to a first approximation we can estimate that in each generation of particles about 25% of the energy is transferred to the electromagnetic shower, and all hadrons with energy $\gtrsim \xi_c^{\pi^\pm}$ interact rather than decay, continuing to produce the hadronic shower. Eventually, the electromagnetic cascade dissipates around 90% of the primary particle's energy and the remaining 10% is carried by muons and neutrinos. Even though these numbers depend on the incident zenith angle of the primary cosmic ray we note that very low energy kaons will decay before interacting to feed the electromagnetic showers in similar way neutral pions do. Therefore, the required symmetry with respect to the CM pseudorapidity seems to indicate that there *must* be swapping of some pions which do not produce an overall effect on the shower evolution. Taking these considerations into account, we are ready to amend the AIRES module.

Before proceeding, we pause to note that we have verified that there is no significant difference in the scattering predictions by changing the hadronic interaction model. For a direct comparison, in Appendix B we show the pion, kaon, and nucleon bivariate distributions for the same particle collisions, but simulated with EPOS-LHC (Pierog et al., 2015).

In what follows we refer to the measurements/tunes performed in the "central" and "forward" regions, as defined with respect to the CM pseudorapidity of the particles. The central pseudorapidity region is defined as $|\eta_{\text{CM}}| \leq 2.5$, corresponding to the ATLAS (Aad et al., 2008), CMS (Chatrchyan et al., 2008) and ALICE (Aamodt et al., 2008) acceptances, and the forward pseudorapidity region as $|\eta_{\text{CM}}| \geq 2.5$. It is generally thought that the observed differences between data and simulation originate, in most part, due to the model extrapolation from the central pseudorapidity region, in which the hadronic event generators adopted in UHECR shower simulations are mainly tuned. We therefore assume herein that the enhancement of strangeness production is negligible for $|\eta_{\text{CM}}| < 4$ (more on this below). The free parameters of the refined model are defined as follows:

Swapping probability $F_s(\eta_{CM})$

Controls the number of secondary pions that are affected by change of identity. F_S depends on the center of mass pseudorapidity of the secondary particles, η_{CM} , and must verify $0 \le F_S \le 1$. Unless otherwise specified, we use

$$F_{s}(\eta_{\text{CM}}) = \begin{cases} f_{s} & \text{if } -\infty < \eta_{\text{CM}} < -4 \\ 0 & \text{if } -4 \le \eta_{\text{CM}} \le 4 \end{cases}, \tag{5}$$

$$f_{s} & \text{if } 4 < \eta_{\text{CM}} < \infty$$

with $0 \le f_s \le 1$.

Minimum projectile energy E_{pmin}

Particle swapping is performed in hadronic collisions whose projectile kinetic energy is larger than this energy. E_{pmin} must be larger than 900 MeV. As in our toy model we take $E_{\text{pmin}} = 1$ PeV.

Minimum secondary energy E_{smin}

Secondary particles with kinetic energies below this threshold are always left unchanged. $E_{\rm smin}$ must be larger than 600 MeV. To sample the entire CM pseudorapidity region we take $E_{\rm smin}=1$ GeV.

The logic of the hadronic collision post-processing remains the same to that discussed in Sec. 2.2.

In Fig. 7 we show $z(R_{\mu})$, $z(\sigma R_{\mu})$, $z(N_{\text{max}})$, and $z(X_{\text{max}})$ as a function of f_s , for E=10 EeV, $E_{\text{smin}}=1$ GeV, and $E_{\text{pmin}}=1$ PeV. We can see that there are no significant changes with respect to the results shown in Fig. 1 for the toy model. It is remarkable that $\forall f_s$ we have $\sigma R_{\mu} < R_{\mu}$, in agreement with Auger observations (Aab et al., 2021). In addition, for the fluctuations of X_{max} (not shown in the figure) we reobtain that $|z(\sigma X_{\text{max}})| < 0.03$ for all $f_s \in [0,1]$. This is because the secondaries emitted in the central pseudorapidity region have minimal impact on the evolution of the shower. This is visible in Fig. 8 where we show $z(R_{\mu})$ as a function of f_s , but with varying limits of the peripheral (pl) and central (cl) regions; namely,

$$F_s^{\text{pl}}(\eta_{\text{CM}}) = \begin{cases} f_s & \text{if } -\infty < \eta_{\text{CM}} < -\eta_{\text{pl}} \\ 0 & \text{if } -\eta_{\text{pl}} \le \eta_{\text{CM}} \le \eta_{\text{pl}} \\ f_s & \text{if } \eta_{\text{pl}} < \eta_{\text{CM}} < \infty \end{cases}$$
(6)

and

$$F_s^{\text{cl}}(\eta_{\text{CM}}) = \begin{cases} 0 & \text{if } -\infty < \eta_{\text{CM}} < -\eta_{\text{cl}} \\ f_s & \text{if } -\eta_{\text{cl}} \le \eta_{\text{CM}} \le \eta_{\text{cl}} \\ 0 & \text{if } \eta_{\text{cl}} < \eta_{\text{CM}} < \infty \end{cases}$$

$$(7)$$

respectively. Moreover, the plots in Fig. 8 clearly show that setting $\eta_{\rm pl} = 3$ or 4 return virtually the same results. For $\eta_{\rm pl} > 4$, the impact of $\pi \to K$ swapping diminish with increasing $\eta_{\rm pl}$, as expected, until presenting a virtually zero impact for $\eta_{\rm pl} = 12$. Complementary, the

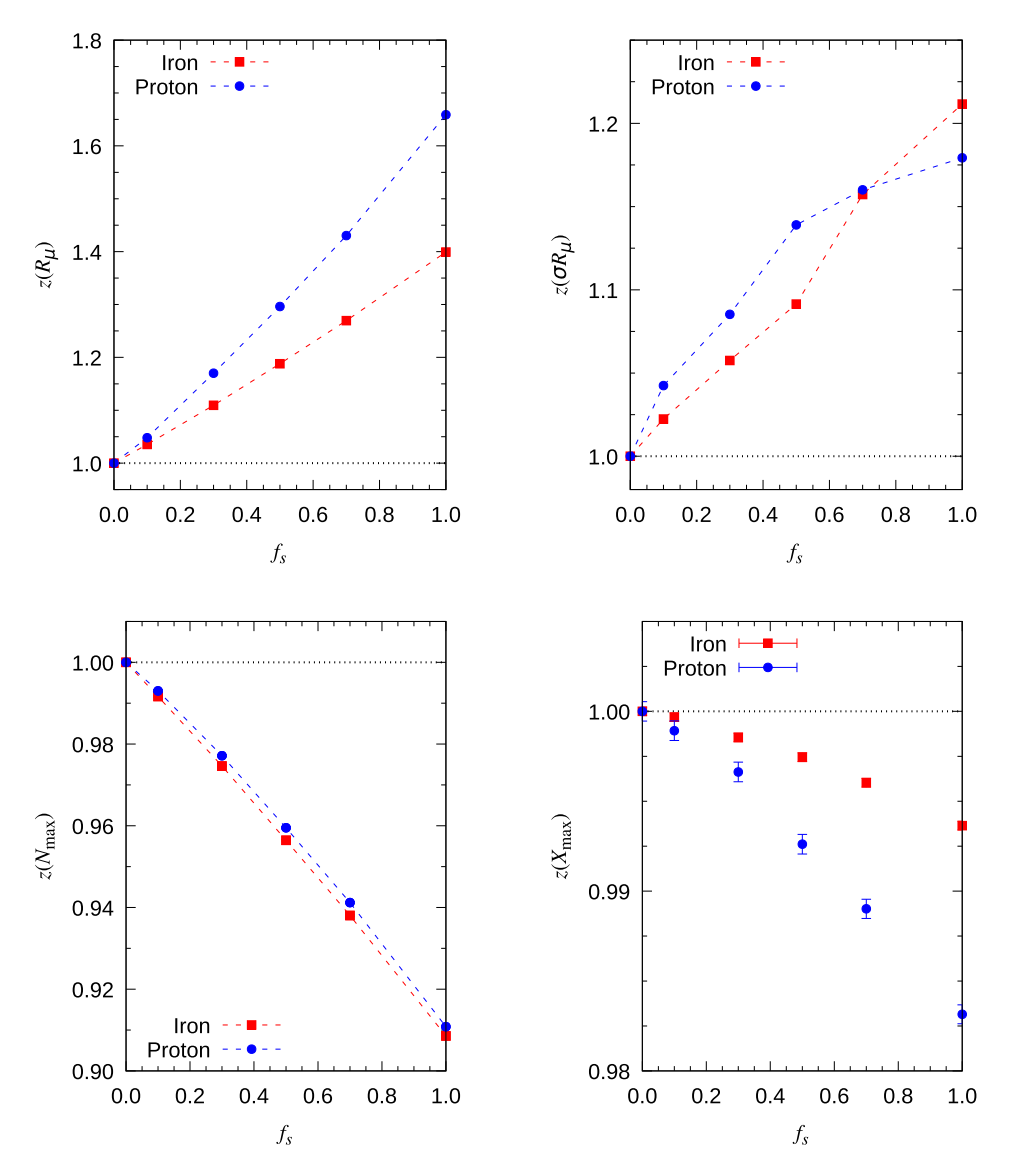


Fig. 7. $z(R_{\mu})$, $z(\sigma R_{\mu})$, $z(\sigma R_{\mu})$, $z(N_{\text{max}})$ and $z(X_{\text{max}})$ as a function of f_s , for $E_{\text{prim}}=10$ EeV, $E_{\text{smin}}=1$ GeV, and $E_{\text{pmin}}=1$ PeV. We have run 8000 (20000) showers per point for ground muons (longitudinal development), setting at each case the thinning algorithm parameters to get a more detailed simulation of the hadronic or the electromagnetic cascade, respectively.

curves displayed in the right panel show that the impact of $\pi \to K$ swapping increases monotonically as long as the "central" region considered gets progressively wider. For $\eta_{cl} < 4$, the central region provides a negligible contribution to $z(R_{\mu})$.

In Fig. 9 we show $\langle R_{\mu} \rangle / (E/10 \text{ EeV})$ considering the variation of UHECR composition shown in Fig. 3 and $F_s(\eta_{CM})$ as defined in Eq. (5). As expected from the discussion above, there is no significant differences with the results displayed in Fig. 3 for the toy model of Sec. 2.

A few crosschecks on these considerations are in order. In Tables 1 and 2 we provide a summary of the global counters of shower simulations using the toy model and the refined model, respectively, with $f_s = 0.7$. It is interesting to note that the percentage of the pions produced above E_{pmin} remains the same and is slightly smaller than 2%. In addition, the number of collisions and consequently the number of secondaries being produced, decreases when considering the refined model. This is because in the toy model we consider

Table 1 Global counters for the toy model with $f_s = 0.7$, in the case of 10^{19} eV proton showers inclined 67° .

Total hadronic collisions per shower Collisions with $E_{\text{proj}} < E_{\text{pmin}}$ Collisions with $E_{\text{proj}} > E_{\text{pmin}}$	287,036 284,374 2.662	100.00% 99.06% 0.94%
Total number of secs. produced Secs. from colls. with $E_{proj} < E_{pmin}$ Secs. from colls. with $E_{proj} > E_{pmin}$	7,315,106 7,036,530 278,576	100.00% 96.19% 3.81%
Total number of pions scanned Pions considered for swapping Pions actually swapped	142,550 56,610 39,609	1.95% 0.77% 0.54%

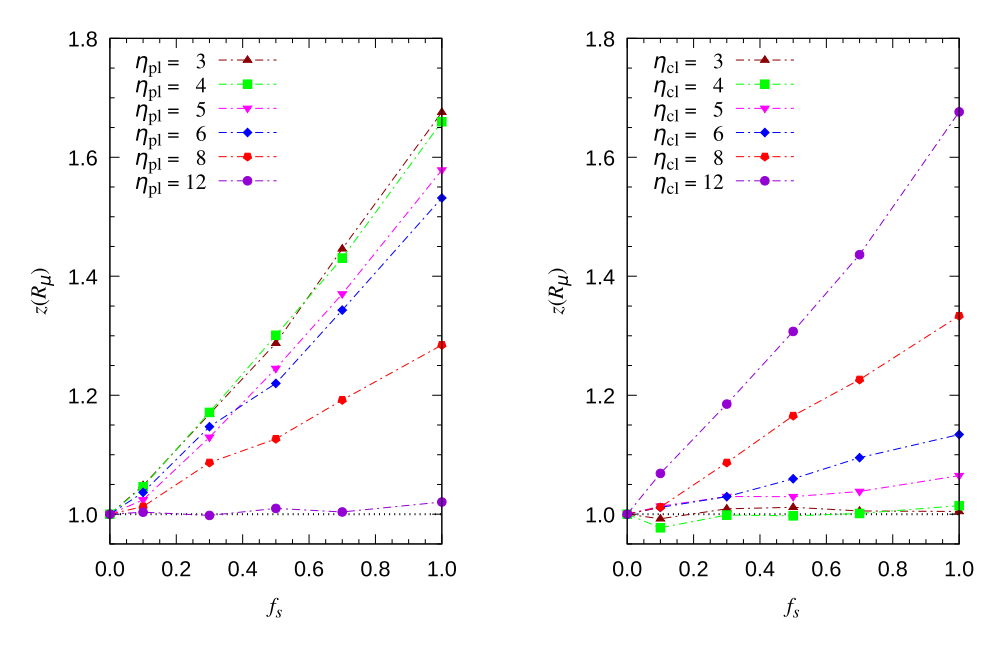


Fig. 8. $z(R_{\mu})$ as a function of f_s , with varying limits of the central (cl) and peripheral (pl) regions. The figure in the left (right) panel compares the results coming from simulations where the swapping algorithm applies to peripheral (central) secondary pions, varying the limits of the peripheral (central) region according to the functions $F_s^{\rm pl}$ and $F_s^{\rm cl}$, defined in Eqs. (6) and (7).

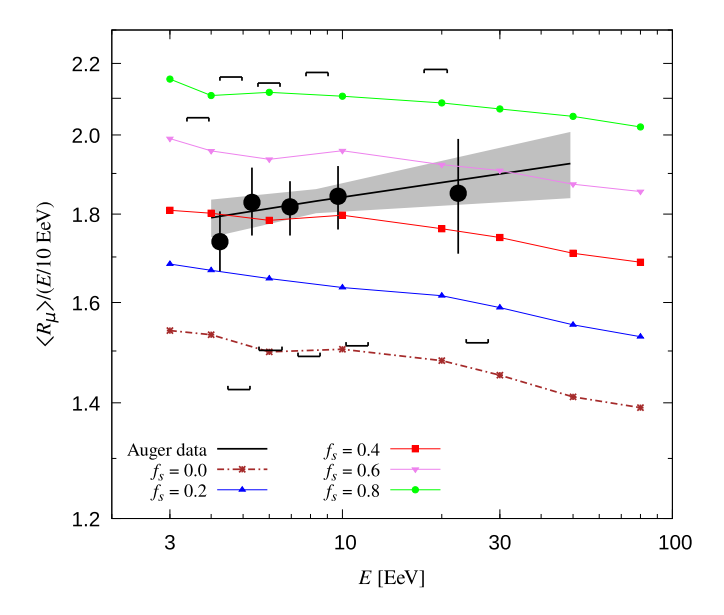


Fig. 9. Estimations of R_{μ} from AIRES simulations for different values of f_s superimposed over Auger data with statistical (ϕ) and systematic (ϕ) uncertainties (Aab et al., 2015). We have adopted the mixed baryonic composition shown in the left panel of Fig. 3.

Table 2 Global counters for the refined model with $f_s=0.7$, in the case of 10^{19} eV proton showers inclined 67° .

Total hadronic collisions per shower	264,600	100.00%
Collisions with $E_{\text{proj}} < E_{\text{pmin}}$	262,070	99.04%
Collisions with $E_{\text{proj}} > E_{\text{pmin}}$	2,530	0.96%
Total number of secs. produced	6,806,244	100.00%
Secs. from colls. with $E_{proj} < E_{pmin}$	6,544,194	96.15%
Secs. from colls. with $E_{\text{proj}} > E_{\text{pmin}}$	262,050	3.85%
Total number of pions scanned	134,060	1.97%
Pions considered for swapping:		
Central $(\eta_{CM} < 4)$	99,790	1.47%
Peripheral $(\eta_{\rm CM} > 4)$	34,270	0.50%
Total (central $+$ peripheral)	134,060	1.97%
Pions actually swapped	23,988	0.35%

secondary neutral pions from the central region with LAB energy above 1 TeV, and if these pions mutate into kaons they would most likely interact before decaying, yielding more collisions in the overall shower and more secondaries. However, the percentage of the number of pions considered for swapping increases in the refined model with a ratio of $40\% \div 96\%$. This is because by lowering the E_{smin} there are many more pions that can be swapped (some of them with $\eta_{CM} < 0$). Looking at the final figures of pions actually swapped, it shows up that the number of swapped pions with respect to the number of scanned pions is more or less the same, and it is actually lower in the refined model; the ratio is $28\% \div 25\%$. The number of swapped pions when compared with the number considered for swapping is roughly 70% in the toy model and reduces to 27% in the refined model. Obviously, the ratio of swapped pions to the *effective* number of pions considered for swapping (i.e., those with $|\eta_{CM}| > 4$) is $f_s = 0.7$. Finally, the number of scanned pions with respect to the total number of secondaries produced with $E_{proj} > E_{pmin}$ is roughly 51%. Note that the fraction of pions produced is larger than 51%, because in the collisions with $E_{proj} \gtrsim E_{pmin}$ there are several pions that have energy below the threshold.

4. Sensitivity to F_s with LHC neutrino experiments

During the next two decades, the LHC will lengthen the energy frontier into both higher energies and much higher luminosities. Most general-purpose LHC detectors, such as ATLAS, CMS, and ALICE are committed to high- p_T physics, featuring events with small cross section: \mathcal{O} (fb, pb, nb). However, the total cross section of LHC collisions is \mathcal{O} (100 mb). Curiously, most of this cross section as well as most of the highest energy particles produced in these collisions are in the far forward region, *viz.* at low p_T . This implies that there is an entire physics program in the far forward region which remains to be explored and can indeed be exploited during the LHC high luminosity (HL) era.

One challenge that far-forward detectors in or close to the LHC beam pipe have to face are the large particle fluxes and radiation levels, essentially restricting their operation to short low-luminosity runs. Another possibility is to make use of the large flux of LHC neutrinos, which can be probed in low-background environments at a safe distance away from the interaction point and accelerator infrastructure. Indeed, the LHC produces an intense and strongly collimated beam of high energy neutrinos in the far-forward direction. These neutrinos are mainly produced in the decay of charged pions, kaons, hyperons and charmed hadrons, making the measurement of the neutrino flux a complimentary probe of forward particle production compared to the neutral pion and neutron measurements performed at LHCf.

The feasibility of such LHC neutrino measurements has recently been demonstrated by the FASER collaboration, which reported the observation of the first neutrino interaction candidates at the LHC (Abreu et al., 2021). Building on this experience, the FASER ν neutrino detector (Abreu et al., 2020, 2001), which is part of the FASER experiment (Feng et al., 2018; Ariga et al., 2018), will start its operation already with the LHC Run 3 in 2022. With a target mass of about 1.2 tons and an anticipated luminosity of 150 fb⁻¹ a total of $\mathcal{O}(10^4)$ muon neutrino and $\mathcal{O}(10^3)$ electron neutrino interactions are expected to be observed. During the HL-LHC, additional far-forward neutrino experiments have been proposed in the context of the FPF (Anchordoqui et al., 2021). In particular, this includes an emulsion based neutrino detector with target mass of about 20 tons called FASER ν 2, a liquid argon based neutrino detector with target mass of about 10 tons called FLATE and an electronic neutrino detector called AdvSND. With their higher target masses and the HL-LHC luminosity of 3000 fb⁻¹ a large event rate of roughly 10^5 electron neutrino and 10^6 muon neutrino interactions is expected to be observed.

Both FASER ν in the near future and the FPF neutrino experiments during the HL-LHC would provide a profitable arena to measure the pion-to-kaon ratio through the shape of differential neutrino flux distributions. In particular, the pion-to-kaon ratio can be inferred by measuring the ratio of electron-to-muon neutrino fluxes. This is because pions primarily decay into muon neutrinos, whereas kaon decays yield a flux of both muon and electron neutrinos. Moreover, neutrinos from different parent mesons populate a different energy range, and so this can be used to disentangle the fluxes. In addition, since $m_{\pi} < m_{K}$, neutrinos from pion decay are more concentrated around the line-of-sight than those of kaon origin, and consequently neutrinos from pions obtain less additional transverse momentum than those from kaon decays. Hence, the closeness of the neutrinos to the line-of-sight, or equivalently their rapidity distribution, becomes a compelling signal to trace back the neutrino origin to measure the pion-to-kaon ratio.

In Fig. 10, we show the expected number of neutrino interactions with the FASER ν detector, assuming a 25 cm \times 25 cm cross sectional area and a 1.2 ton target mass, as a function of the neutrino energy. Here, we have used SIBYLL 2.3d (Riehn et al., 2020) as primary generator and use the fast LHC neutrino flux simulation introduced by Kling and Nevay (2021) to describe the propagation and decay the long-lived hadrons in the LHC beam pipe. The origin of the neutrinos is indicated by the different line colors: red for pion decay, blue for kaon decay, magenta for hyperon decay, and green for charm decay. As explained above, the neutrinos from pions and kaons populate different regions of phase space, which can be used to disentangle pion and kaon production. In Fig. 11, we also show the results for the FLATE detector at the FPF, which is assumed to have a 1 m \times 1 m cross sectional area and a 10 ton target mass.

In Fig. 10 and Fig. 11, we also show how a $\pi \leftrightarrow K$ swapping as defined in Eq. (5) changes the expected neutrino fluxes and event rates for the considered experiments. As expected, positive values of f_s lead to a suppression of the neutrino flux from pions as well as a larger relative enhancement of the neutrino flux from kaons. This is due to the initially roughly 10 times larger flux of pions, such that even a small rate of $\pi \leftrightarrow K$ swapping can substantially increase the neutrino flux from the kaon decays. This leads to the remarkable result that already for $f_s = 0.1$ ($f_s = 0.2$) the predicted electron neutrino flux at the peak of the spectrum is a factor of 1.6 (2.2) larger. These differences are significantly larger than the anticipated statistical uncertainties at the FPF (Kling and Nevay, 2021; Anchordoqui et al., 2021). This lets us conclude that LHC neutrino flux measurements with new forward detectors at the LHC will provide invaluable complementary information to test our model and its improvements, together with eventual alternative ones, addressing the muon puzzle via strangeness enhancement.

5. Conclusions

We have examined the influence of $\pi \leftrightarrow K$ swapping on the development of extensive air showers. We constructed an empirical testable model, based on ALICE observations of the enhancement of strangeness production in high-energy hadronic collisions, which can

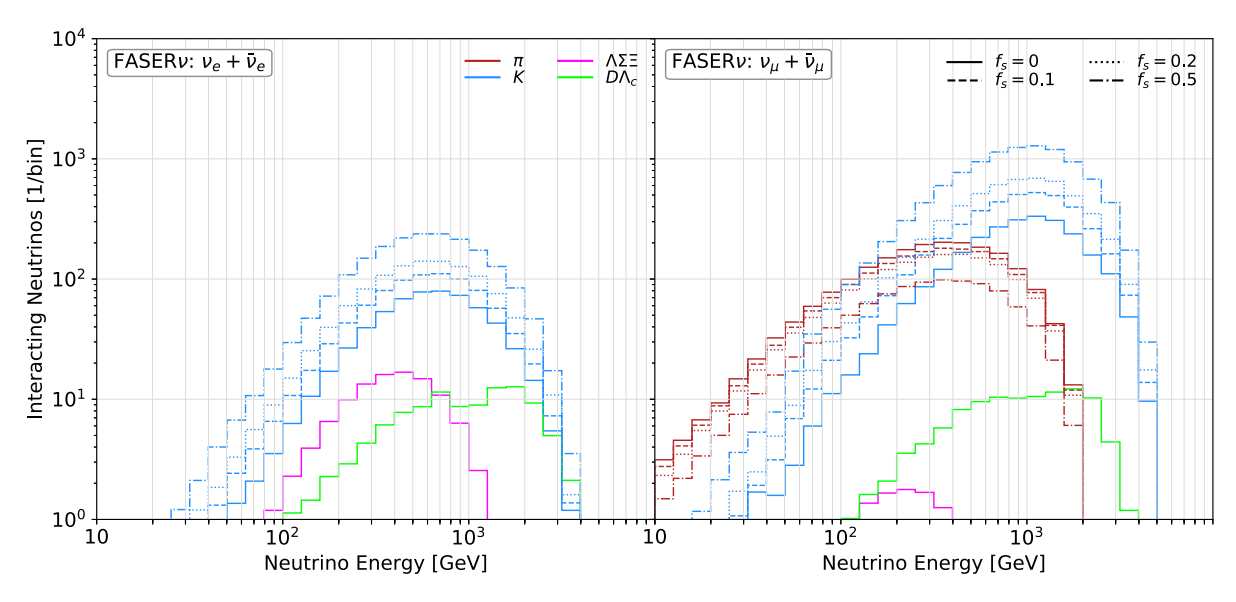


Fig. 10. Energy spectrum of neutrinos (left) and muon neutrinos (right) interacting with FASER ν . The vertical axis shows the number of charged current neutrino interactions per energy bin for an integrated luminosity of 150 fb⁻¹ by different colors: pion decays (red), kaon decays (blue), hyperon decays (magenta), and charm decays (green). The different line styles correspond to predictions obtained from SIBYLL-2.3d with secondary pions processed using the refined model with $F_s(\eta_{CM})$ as in Eq. (5), for different values of f_s .

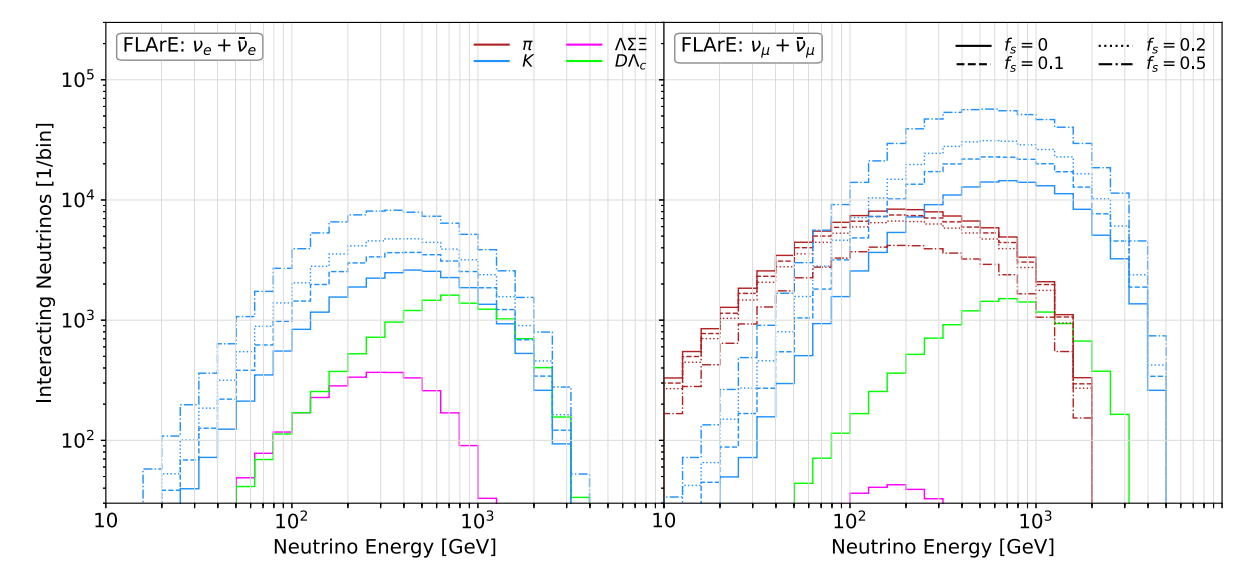


Fig. 11. Expected number of charged current neutrino interactions with the FLArE detector at the FPF assuming an integrated luminosity of 3 ab⁻¹. See Fig. 10 for details.

accommodate the muon deficit between simulations and Auger data. We derived a parametrization of the $\pi \leftrightarrow K$ swapping probability in terms of the pseudorapidity and the nucleus baryon number.

We have also explored potential strategies for model improvement using the massive amounts of data to be collected at the FASER ν and future LHC neutrino experiments at the FPF. We have shown that these experiments will attain sensitivity to probe the model phase space.

Within this decade, ongoing detector upgrades of existing facilities, such as AugerPrime (Aab et al., 2016b) and IceCube-Gen2 (Aartsen et al., 2021), will enhance the precision of air shower measurements and reduce uncertainties in the interpretation of muon data. In particular, as a part of the upcoming AugerPrime upgrade each surface station will have additional detectors that will provide complementary measurements of the incoming shower particles, consequently leading to improved reconstruction of muons and electromagnetic particles (Aab et al., 2016b). This will allow for the measurement of the properties of extensive air showers initiated by the highest energy cosmic rays with unprecedented precision. As we have shown in this paper, future Auger measurements will be highly complemented by observations at the LHC neutrino experiments which will provide a unique determination of the pion-to-kaon ratio at LHC energies. Altogether this will provide a powerful test of models addressing the muon puzzle via strangeness enhancement.

¹ One possible realization of our phenomenological model may be obtained by considering collective statistical hadronization effects into the standard string fragmentation process (Baur et al., 2019).

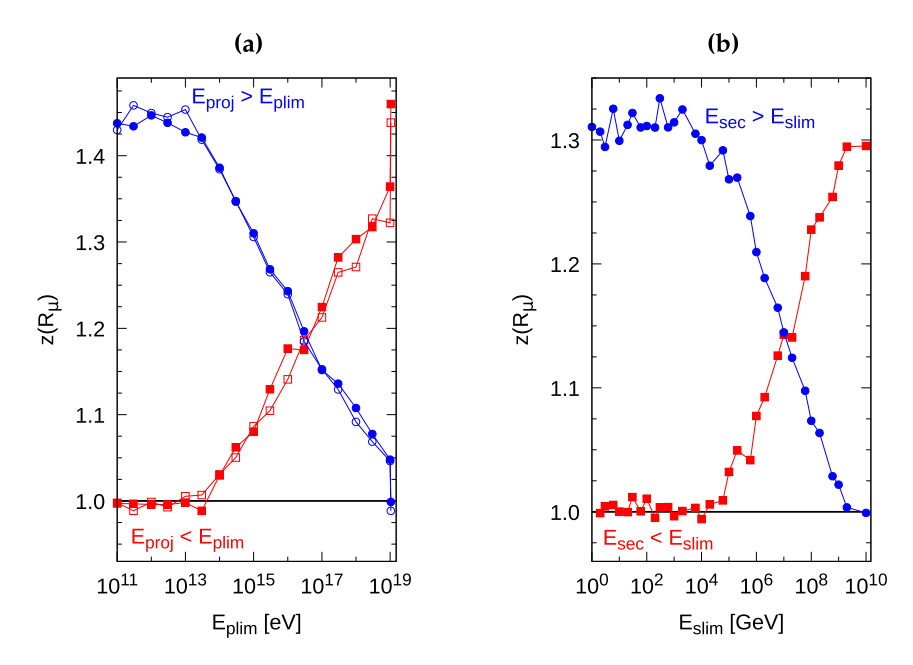


Fig. 12. $z(R_{\mu})$ as a function of E_{plim} (a) and E_{slim} (b) for fixed $f_s = 0.5$. (a) Varying projectile energy range, with fixed secondary energy range. $[E_{\text{smin}}, E_{\text{smax}}]$ is always kept fixed and equal to $[1 \text{ TeV}, \infty]$ (solid symbols) or $[1 \text{ GeV}, \infty]$ (open symbols). Each blue circle (red square) in the figure corresponds to simulations run with $[E_{\text{pmin}}, E_{\text{pmax}}] = [E_{\text{plim}}, E_{\text{pmax}}] = [E_{\text{plim}}, E_{\text{pmax}}] = [E_{\text{pmin}}, E_{\text{pmax}}] = [E_{\text{p$

Declaration of competing interest

The authors declare that they have no known competing financial interests or personal relationships that could have appeared to influence the work reported in this paper.

Acknowledgments

We thank our colleagues from the Pierre Auger Collaboration for valuable discussion. L.A.A. and J.F.S. are supported by U.S. National Science Foundation (NSF Grant PHY-2112527). C.G.C. and S.J.S. are partially supported by ANPCyT. The work of F.K. is supported by the Deutsche Forschungsgemeinschaft under Germany's Excellence Strategy - EXC 2121 Quantum Universe - 390833306.

Appendix A. Limiting projectile and secondary energies

In this Appendix we analyze the variation of $z(R_{\mu})$ with both projectile and secondary energies for fixed f_s . To this end we introduce the new variables E_{plim} and E_{slim} to limit the maximum and minimum energies of the projectile E_{proj} and secondary E_{sec} , respectively. In Fig. 12 we show $z(R_{\mu})$ as a function of E_{plim} and E_{slim} , for fixed $f_s = 0.5$. By analyzing the variation of $z(R_{\mu})$ with E_{plim} and E_{slim} we conclude that:

- The impact of the substitution of π 's by K's reaches a maximum when $0 < E_{pmin} \lesssim 10$ TeV.
- In (a), at $E_{\text{plim}} \simeq 10^{19}$ eV, both the blue and red sets show pairs of points significantly apart: they correspond to values of E_{plim} slightly smaller or larger than the primary energy (10¹⁹ eV), that respectively prevents or not the application of the swapping algorithm to the first hadronic interaction at the beginning of the shower development. This reveals that the first interaction has, by itself, a finite impact of the final number of muons at ground.
- There are no significant differences between the open and solid symbols plots included in (a). This means that swapping of low energy pions (E_{sec} lower than 1 TeV) has no visible impact on $z(R_{\mu})$. This also shows up clearly in (b) where the blue points remain around the maximum value for $E_{\text{slim}} \lesssim 1$ TeV.

Appendix B. EPOS-LHC

In this Appendix we report on the results of simulated particle collisions with EPOS-LHC (Pierog et al., 2015). In Fig. 13 we show bivariate distributions of secondary pions. From a comparison with Fig. 5 we see that there are no major differences in the distributions, but just a small deviation of the predicted multiplicity in the central region.

We have shown elsewhere (Sciutto, 2019) that the discrepancy between Auger data and air shower simulations with SIBYLL 2.3d is slightly smaller than the discrepancy obtained from simulations with EPOS-LHC 1909. For showers process with QGSJetII-04 hadronic event generator (Ostapchenko, 2011), the discrepancy between data and simulations is even larger (Aab et al., 2016a). This justifies the choice of SIBYLL 2.3d in our study.

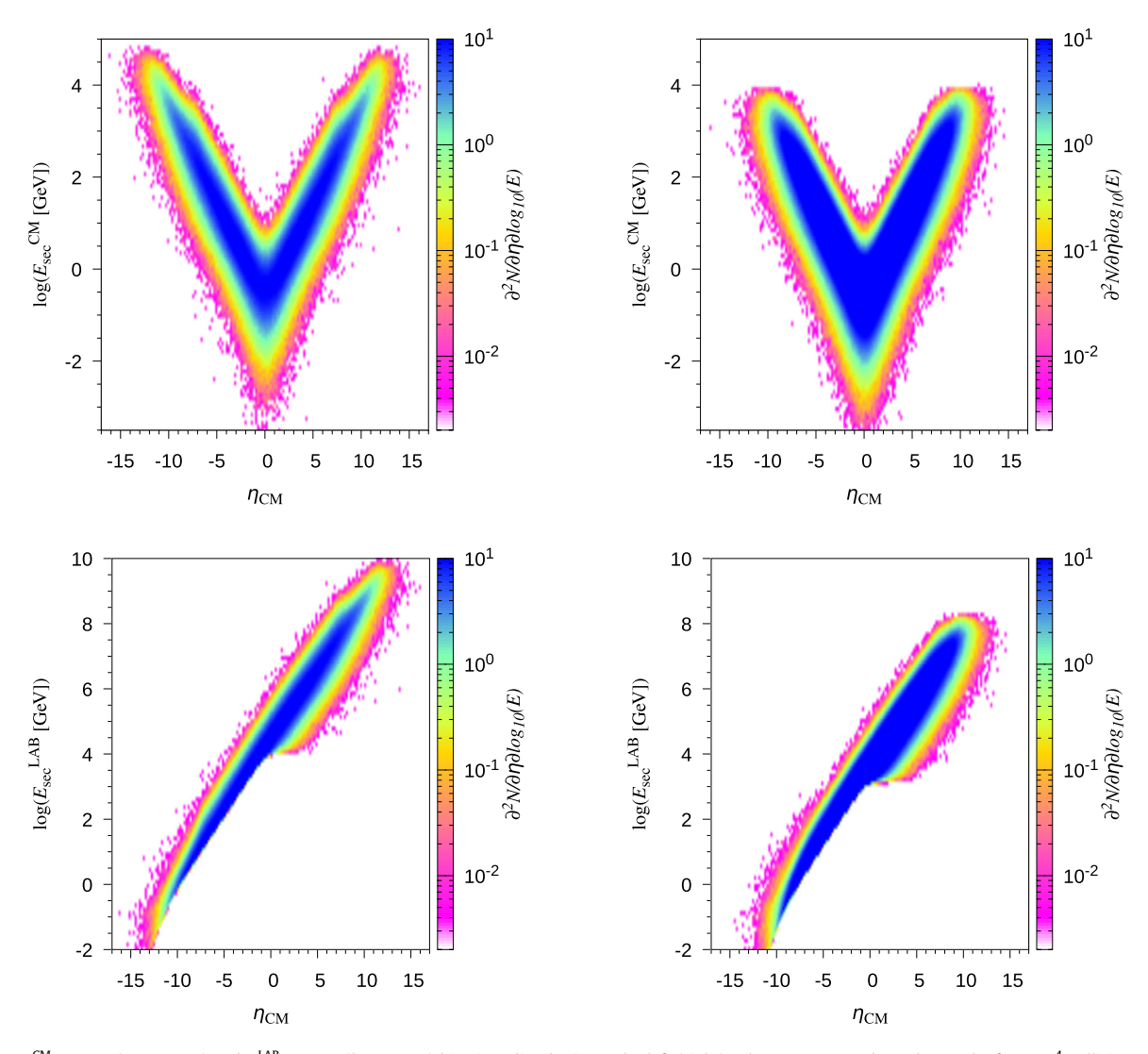


Fig. 13. Pion $E_{\text{sec}}^{\text{CM}}$ vs η_{CM} (upper row) and $E_{\text{sec}}^{\text{LAB}}$ vs η_{CM} (lower row) bivariate distributions. The left (right) column corresponds to the results from 10^4 collisions of a 10 EeV proton (iron nucleus) scattering off a proton (nitrogen nucleus) at rest, simulated with EPOS-LCH 1909.

References

Aab, A., et al., Pierre Auger Collaboration, 2015. Muons in air showers at the Pierre Auger Observatory: mean number in highly inclined events. Phys. Rev. D 91 (3), 032003. https://doi.org/10.1103/PhysRevD.91.032003. Erratum: Phys. Rev. D 91 (5), 059901. https://doi.org/10.1103/PhysRevD.91.059901 (2015). arXiv:1408.1421 [astro-ph.HE]. Aab, A., et al., Pierre Auger Collaboration, 2016a. Testing hadronic interactions at ultrahigh energies with air showers measured by the Pierre Auger Observatory. Phys. Rev. Lett. 117, 192001. https://doi.org/10.1103/PhysRevLett.117.192001. arXiv:1610.08509 [hep-ex].

Aab, A., et al., Pierre Auger Collaboration, 2016b. The Pierre Auger Observatory upgrade: preliminary design report. arXiv:1604.03637 [astro-ph.IM].

Aab, A., et al., Pierre Auger Collaboration, 2017. Combined fit of spectrum and composition data as measured by the Pierre Auger Observatory. J. Cosmol. Astropart. Phys. 04, 038. https://doi.org/10.1088/1475-7516/2017/04/038. Erratum: J. Cosmol. Astropart. Phys. 03, E02 (2018). arXiv:1612.07155 [astro-ph.HE].

Aab, A., et al., Pierre Auger Collaboration, 2021. Measurement of the fluctuations in the number of muons in extensive air showers with the Pierre Auger Observatory. Phys. Rev. Lett. 126 (15), 152002. https://doi.org/10.1103/PhysRevLett.126.152002. arXiv:2102.07797 [hep-ex].

Aad, G., et al., ATLAS Collaboration, 2008. The ATLAS experiment at the CERN Large Hadron Collider. J. Instrum. 3, S08003. https://doi.org/10.1088/1748-0221/3/08/S08003. Aamodt, K., et al., ALICE Collaboration, 2008. The ALICE experiment at the CERN LHC. J. Instrum. 3, S08002. https://doi.org/10.1088/1748-0221/3/08/S08002.

Aartsen, M.G., et al., IceCube-Gen2 Collaboration, 2021. IceCube-Gen2: the window to the extreme Universe. J. Phys. G 48 (6), 060501. https://doi.org/10.1088/1361-6471/abbd48. arXiv:2008.04323 [astro-ph.HE].

Abbasi, R.U., et al., Telescope Array Collaboration, 2018. Study of muons from ultrahigh energy cosmic ray air showers measured with the Telescope Array experiment. Phys. Rev. D 98 (2), 022002. https://doi.org/10.1103/PhysRevD.98.022002. arXiv:1804.03877 [astro-ph.HE].

Abelev, B.B., et al., ALICE Collaboration, 2014. Multi-strange baryon production at mid-rapidity in Pb-Pb collisions at $\sqrt{s_{NN}}$ = 2.76 TeV. Phys. Lett. B 728, 216–227. https://doi.org/10.1016/j.physletb.2014.05.052. Erratum: Phys. Lett. B 734, 409–410 (2014). arXiv:1307.5543 [nucl-ex].

Abreu, H., et al., FASER, 2001. Technical proposal: FASERv. arXiv:2001.03073 [physics.ins-det].

Abreu, H., et al., FASER, 2020. Detecting and studying high-energy collider neutrinos with FASER at the LHC. Eur. Phys. J. C 80 (1), 61. https://doi.org/10.1140/epjc/s10052-020-7631-5. arXiv:1908.02310 [hep-ex].

Abreu, H., et al., FASER, 2021. First neutrino interaction candidates at the LHC. Phys. Rev. D 104 (9), L091101. https://doi.org/10.1103/PhysRevD.104.L091101. arXiv:2105.06197 [hep-ex].

Adam, J., et al., ALICE Collaboration, 2017. Enhanced production of multi-strange hadrons in high-multiplicity proton-proton collisions. Nat. Phys. 13, 535. https://doi.org/10.1038/nphys4111. arXiv:1606.07424 [nucl-ex].

Adriani, O., et al., LHCf Collaboration, 2014. Transverse-momentum distribution and nuclear modification factor for neutral pions in the forward-rapidity region in proton-lead collisions at $\sqrt{s_{NN}} = 5.02$ TeV. Phys. Rev. C 89 (6), 065209. https://doi.org/10.1103/PhysRevC.89.065209. arXiv:1403.7845 [nucl-ex]. Allen, J., Farrar, G., 2013. Testing models of new physics with UHE air shower observations. arXiv:1307.7131 [astro-ph.HE].

Anchordoqui, L.A., 2019. Ultra-high-energy cosmic rays. Phys. Rep. 801, 1-93. https://doi.org/10.1016/j.physrep.2019.01.002, arXiv:1807.09645 [astro-ph.HE].

Anchordoqui, L.A., Goldberg, H., Weiler, T.J., 2017. Strange fireball as an explanation of the muon excess in Auger data. Phys. Rev. D 95 (6), 063005. https://doi.org/10.1103/PhysRevD.95.063005. arXiv:1612.07328 [hep-ph].

Anchordoqui, L.A., García Canal, C., Sciutto, S.J., Soriano, J.F., 2020. Through the looking-glass with ALICE into the quark-gluon plasma: a new test for hadronic interaction models used in air shower simulations. Phys. Lett. B 810, 135837, https://doi.org/10.1016/j.physletb.2020.135837, arXiv:1907.09816 [hep-ph].

Anchordoqui, L.A., et al., 2021. The Forward Physics Facility: sites, experiments, and physics potential. arXiv:2109.10905 [hep-ph].

Ariga, A., et al., FASER Collaboration, 2018. Technical proposal for FASER: ForwArd Search ExpeRiment at the LHC. arXiv:1812.09139 [physics.ins-det].

Baur, S., Dembinski, H., Perlin, M., Pierog, T., Ulrich, R., Werner, K., 2019. Core-corona effect in hadron collisions and muon production in air showers. arXiv:1902.09265 [hep-ph].

Chatrchyan, S., et al., CMS Collaboration, 2008. The CMS experiment at the CERN LHC. J. Instrum. 3, S08004. https://doi.org/10.1088/1748-0221/3/08/S08004.

Citron, Z., et al., 2019. Report from Working Group 5: Future physics opportunities for high-density QCD at the LHC with heavy-ion and proton beams. CERN Yellow Rep. Monogr. 7, 1159–1410. https://doi.org/10.23731/CYRM-2019-007.1159. arXiv:1812.06772 [hep-ph].

Dembinski, H., Albrecht, J., Cazon, L., Fedynitch, A., Kampert, K.H., Pierog, T., Rhode, W., Soldin, D., Spaan, B., Ulrich, R., Unger, M., 2021. The muon puzzle in air showers and its connection to the LHC. PoS ICRC2021, 037. https://doi.org/10.22323/1.395.0037. arXiv:2105.06148 [astro-ph.HE].

d'Enterria, D., Engel, R., Pierog, T., Ostapchenko, S., Werner, K., 2011. Constraints from the first LHC data on hadronic event generators for ultra-high energy cosmic-ray physics. Astropart. Phys. 35, 98–113. https://doi.org/10.1016/j.astropartphys.2011.05.002. arXiv:1101.5596 [astro-ph.HE].

Farrar, G.R., Allen, J., 2013. Evidence for some new physical process in ultrahigh-energy collisions. EPJ Web Conf. 52, 07005. https://doi.org/10.1051/epjconf/20125207005. Feng, J.L., Galon, I., Kling, F., Trojanowski, S., 2018. ForwArd Search ExpeRiment at the LHC. Phys. Rev. D 97 (3), 035001. https://doi.org/10.1103/PhysRevD.97.035001. arXiv: 1708.09389 [hep-ph].

Gondolo, P., Ingelman, G., Thunman, M., 1996. Charm production and high-energy atmospheric muon and neutrino fluxes. Astropart. Phys. 5, 309–332. https://doi.org/10. 1016/0927-6505(96)00033-3. arXiv:hep-ph/9505417 [hep-ph].

Kling, F., Nevay, L.J., 2021. Forward neutrino fluxes at the LHC. arXiv:2105.08270 [hep-ph].

Ostapchenko, S., 2011. Monte Carlo treatment of hadronic interactions in enhanced Pomeron scheme I: QGSJET-II model. Phys. Rev. D 83, 014018. https://doi.org/10.1103/PhysRevD.83.014018. arXiv:1010.1869 [hep-ph].

Palni, P., for the ALICE Collaboration, 2019. Multiplicity dependence of strangeness and charged particle production in proton-proton collisions. Acta Phys. Pol. B 50, 1185. https://doi.org/10.5506/APhysPolB.50.1185. arXiv:1904.00005 [nucl-ex].

Pierog, T., Karpenko, I., Katzy, J.M., Yatsenko, E., Werner, K., 2015. EPOS LHC: test of collective hadronization with data measured at the CERN Large Hadron Collider. Phys. Rev. C 92 (3), 034906. https://doi.org/10.1103/PhysRevC.92.034906. arXiv:1306.0121 [hep-ph].

Riehn, F., Engel, R., Fedynitch, A., Gaisser, T.K., Stanev, T., 2020. Hadronic interaction model Sibyll 2.3d and extensive air showers. Phys. Rev. D 102 (6), 063002. https://doi.org/10.1103/PhysRevD.102.063002. arXiv:1912.03300 [hep-ph].

Sciutto, S.J., 1999. AIRES: a system for air shower simulations. arXiv:astro-ph/9911331. http://aires.fisica.unlp.edu.ar.

Sciutto, S.J., 2019. Air showers, hadronic models, and muon production. EPJ Web Conf. 210, 02007. https://doi.org/10.1051/epjconf/201921002007. arXiv:1904.12056 [astro-ph.HE].

Zyla, P.A., et al., Particle Data Group, 2020. Review of Particle Physics. PTEP 2020 (8), 083C01. https://doi.org/10.1093/ptep/ptaa104.